

Kerker scattering of electrons: Towards futuristic thermoelectric materials

Mahdiyeh Sadrara

*School of Nano Science, Institute for Research in Fundamental Sciences (IPM), P.O. Box 19395-5531, Tehran, Iran*MirFaez Miri ^{*}*Department of Physics, University of Tehran, P.O. Box 14395-547, Tehran, Iran* (Received 31 July 2022; revised 21 August 2022; accepted 29 August 2022; published 8 September 2022)

Historically, the transfer of ideas and concepts between optics and condensed-matter physics has been flourishing. Inspired by shaping the scattering of electromagnetic waves by dielectric nanoparticle clusters through the interference of excited multipole modes, we address shaping the scattering of matter waves by quantum dot clusters embedded in a host semiconductor through the interference of excited partial waves. We theoretically demonstrate nearly complete suppression of backward, forward, and both backward and forward scattering, i.e., three versions of the generalized Kerker scattering of matter waves. We envisage that thermoelectric properties of semiconductors can be improved by incorporation of quantum dot clusters exhibiting ultradirectional forward scattering: Such clusters act as phonon-blocking/electron-transmitting inclusions.

DOI: [10.1103/PhysRevB.106.115201](https://doi.org/10.1103/PhysRevB.106.115201)**I. INTRODUCTION**

Nanophotonics, the science of controlling the interaction of light and matter on subwavelength scales, has experienced an explosive growth in the past two decades [1,2]. Metallic nanoparticles have attracted much attention in this field. Metallic nanoparticles derive their fascinating properties from an ability to support collective electron excitations, known as localized surface plasmons. Using metallic nanoparticles, nanoscale optical devices such as nanolenses [3], nanowaveguides [4,5], and nanoantennas [6] are realized. Indeed only the *electric* response of such metallic nanostructures is engineered to control and shape the scattering pattern.

As early as 1983, Kerker, Wang, and Giles discovered peculiarities of electromagnetic plane wave scattering by *magnetic* spherical particles [7]: Under certain conditions for the values of the electric permittivity ϵ and magnetic permeability μ , the induced electric and magnetic dipoles are of equal magnitude, and consequently the in-phase and out-of-phase oscillation of these induced dipoles leads to the zero-backward (first Kerker condition) and near-zero-forward (second Kerker condition) radiated power, respectively. The Kerker conditions are indeed too restrictive since most natural materials exhibit no considerable magnetic response, i.e., $\mu \approx 1$, especially in the visible region of the spectrum. Therefore, electromagnetic scattering by magnetodielectric spherical particles faded into oblivion.

The theoretical prediction and experimental realization of double-negative metamaterials operating in the microwave region coined the concept of artificial magnetism [8,9]. Now it is well known that high-index dielectric nanoparticles offer a route to considerable magnetic response in the visible

spectral range [10–12]: According to the Mie theory, high-index dielectric nanoparticles can exhibit strong magnetic dipole resonance, due to the circular displacement current excited by the incident wave. Intriguingly, the response of the excited magnetic dipole may become comparable to or even stronger than that of the excited electric dipole. Recognition of the interference of electric and magnetic multipolar resonances in high-index dielectric nanoparticles revitalized the Kerker scattering [13–16]. Shaping the scattering pattern beyond the forward and backward directions has also been discussed. Particularly, nearly complete simultaneous suppression of both forward and backward scattering, the so-called transverse Kerker scattering, has gained interest [17–22]. Kerker scattering and transverse Kerker scattering by a dielectric nanoparticle are experimentally confirmed [13,14,19]. Directional scattering from nanoparticle clusters such as dimers [23–25], trimers [23,26,27], and quadrumers [23] is studied. Moreover, meta-atoms supporting the transverse Kerker effect are arranged into a lattice to realize extraordinarily *transparent* metasurfaces: At the resonant frequency, the transmitted light traverses the metasurface without perturbation of its amplitude and phase [28]. Note that in Huygens' metasurfaces, the strong forward scattering leads to a phase difference between the incident and transmitted fields.

Since the milestone experiments of Davisson and Germer, and Thomson, there is a tradition in highlighting the similarities between wave optics and wave mechanics. In this respect, the transfer of ideas and concepts between optics and condensed-matter physics has been flourishing [29], as exemplified by the invention of photonic crystals, Anderson localization of light, topological photonics, the multi-quantum-well barrier to reflect incident electrons [30], the electronic Mach-Zehnder interferometer to measure interference of quasiparticles with fractional charges [31], and cloaking a quantum dot from impinging matter waves based

*mirfaez_miri@ut.ac.ir

on an analog of plasmonic cloaking of electromagnetic waves [32–40].

In this paper, we theoretically demonstrate Kerker scattering and transverse Kerker scattering of *matter waves* by one or a cluster of spherical core-shell quantum dots embedded in a host semiconductor. In general, these quantum dots are not arranged in a regular pattern and thus the potential felt by the electron is not spherically symmetric. Guided by the multiparticle Mie theory [41], we present a generalized partial wave method to treat the electron multiple scattering. The electron scattering pattern not only depends on each quantum dot characteristic—i.e., radius, effective mass, and potential of the core/shell—but also on the geometrical arrangement of quantum dots. We show that with a proper choice of parameters, the *interference* of *s*, *p*, *d*, and even *f* waves, and consequently the scattering pattern, can be engineered.

There is at least one good reason to engineer electron scattering from quantum dots which are interchangeably called nanoinclusions and nanoparticles. Regarding the increasing need for clean energy resources, and the estimation that 72% of the global primary energy consumption is lost after conversion [42], thermoelectric devices which generate electricity from waste heat are of paramount importance [43]. However, the relatively low energy conversion efficiency of conventional thermoelectrics has limited their use. Thus intense research is focused on new bulk and thin-film thermoelectric materials, and even few-layer and single-layer two-dimensional materials such as graphene, black phosphorus, transition-metal dichalcogenides, group IV–VI compounds, and MXenes [44,45]. Recent experiments have confirmed that thermoelectric properties of semiconductors can be improved by incorporation of nanoinclusions [46–49]. Such so-called phonon-blocking/electron-transmitting nanoinclusions are believed to strongly scatter phonons while not severely deteriorating electron transport. At low concentrations of nanoinclusions, scattering events are almost independent. But at high concentrations of nanoinclusions >1%, electron multiple scatterings are important [50]. Along these lines, cloaking *one* core-shell nanoparticle from conducting electrons is discussed [32,33]. However, *collective* cloaking of a cluster of quantum dots is rather involved [40]. In this respect, we pay attention to the ultradirectional forward scattering by a cluster of quantum dots. We also envisage a new generation of quantum dot superlattice thermoelectric materials based on quantum dots supporting the transverse Kerker effect: Indeed “transverse scatterers” arranged into a lattice are expected to be *transparent* to matter waves.

II. MODEL

We study the multiple scattering of an electron from N core-shell quantum dots embedded in a host semiconductor. In general, these spherical quantum dots are not arranged in a regular pattern. In other words, the scattering potential is not spherically symmetric (see Fig. 1). We rely on the effective-mass Hamiltonian

$$H = -\frac{\hbar^2}{2} \nabla \cdot \frac{1}{m(\mathbf{r})} \nabla + V(\mathbf{r}) \quad (1)$$

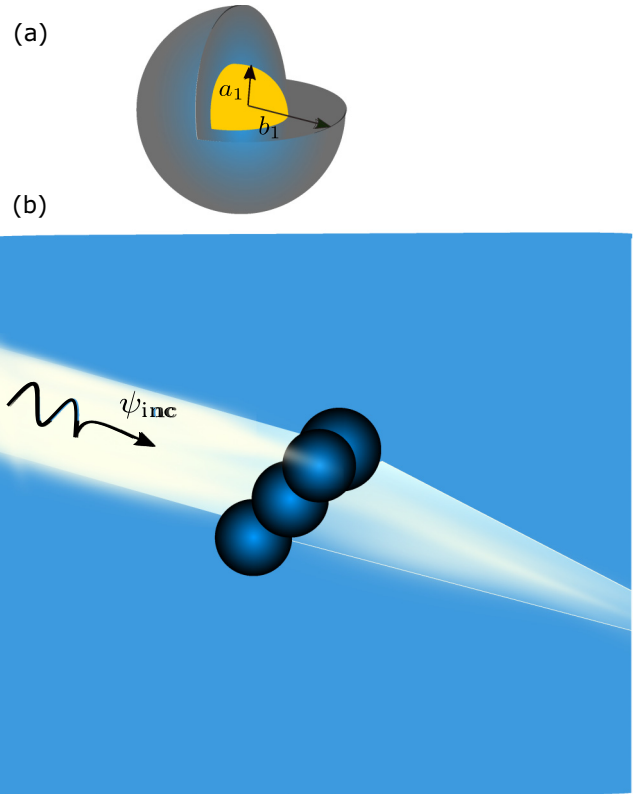


FIG. 1. (a) Schematics of a core-shell quantum dot with inner radius a_1 and outer radius b_1 . (b) An artistic view of electron wave scattering from a cluster of core-shell quantum dots.

to describe the electron dynamics. The effective mass in the host semiconductor m_h , wave number k , wave vector $\mathbf{k} = k\hat{z}$, and energy $E = \hbar^2 k^2 / (2m_h)$ characterize the incident electron. The wave function of the incident electron is $\psi_{\text{inc}} = e^{ikz}$. The center O_α , position \mathbf{d}_α , radius a_α , effective mass $m_{c,\alpha}$, and band offset with respect to the host semiconductor, or potential $V_{c,\alpha}$ of the core region $|\mathbf{r} - \mathbf{d}_\alpha| < a_\alpha$, radius b_α , effective mass $m_{s,\alpha}$, and potential $V_{s,\alpha}$ of the shell region $a_\alpha < |\mathbf{r} - \mathbf{d}_\alpha| < b_\alpha$, characterize the α th spherical quantum dot. We use $\bar{a} = (\frac{1}{N} \sum_{\alpha=1}^N a_\alpha^2)^{1/2}$ and $\bar{b} = (\frac{1}{N} \sum_{\alpha=1}^N b_\alpha^2)^{1/2}$ as the typical inner and outer radii, respectively.

III. ELECTRON SCATTERING FROM ONE QUANTUM DOT

First we revisit electron scattering from *one* core-shell quantum dot centered at the origin of the coordinates [34]. The Hamiltonian H commutes with the angular momentum operators L^2 and L_z . Thus it is convenient to invoke the simultaneous eigenfunctions of L^2 and L_z , i.e., the spherical harmonics $Y_{lm}(\hat{\mathbf{r}})$, to construct the eigenfunctions of H . Indeed the incident plane wave can be expanded as

$$\psi_{\text{inc}} = e^{ikz} = \sum_{l=0}^{\infty} i^l \sqrt{4\pi(2l+1)} j_l(kr) Y_{l0}(\theta, \phi). \quad (2)$$

The transmitted waves $\psi_{\text{core},1}$ and $\psi_{\text{shell},1}$, and the scattered wave ψ_{sca} , can be expanded as well,

$$\begin{aligned}\psi_{\text{core},1} &= \sum_{l=0}^{\infty} i^l \sqrt{4\pi(2l+1)} T_{l,1}^c j_l(q_{c,1}r) Y_{l0}(\theta, \phi), \\ \psi_{\text{shell},1} &= \sum_{l=0}^{\infty} i^l \sqrt{4\pi(2l+1)} [T_{l,1}^s j_l(q_{s,1}r) \\ &\quad + T_{l,1}^{s'} y_l(q_{s,1}r)] Y_{l0}(\theta, \phi), \\ \psi_{\text{sca}} &= \sum_{l=0}^{\infty} i^l \sqrt{4\pi(2l+1)} R_{l,1} h_l^{(1)}(kr) Y_{l0}(\theta, \phi).\end{aligned}\quad (3)$$

Here angular momentum quantum numbers $l = 0, 1, 2, 3, 4, 5, \dots$ specify s, p, d, f, g, h, \dots partial mat-

ter waves. j_l, y_l , and $h_l^{(1)} = j_l + iy_l$ denote the spherical Bessel, spherical Neumann, and spherical Hankel functions of the first kind, respectively. $q_{c,\alpha} = \frac{\chi_{c,\alpha}}{\hbar} \sqrt{2m_{c,\alpha}|E - V_{c,\alpha}|}$, $q_{s,\alpha} = \frac{\chi_{s,\alpha}}{\hbar} \sqrt{2m_{s,\alpha}|E - V_{s,\alpha}|}$, $\chi_{c/s,\alpha} = 1$ if $E - V_{c/s,\alpha} \geq 0$ and $\chi_{c/s,\alpha} = i$ if $E - V_{c/s,\alpha} < 0$. Note that the above wave functions have no dependence on the azimuthal angle ϕ , due to the rotational invariance of the system about the \hat{z} axis.

At the interface of two regions I and II, the probability amplitude and the current are continuous. It follows that the boundary conditions at the interface are $\psi_I = \psi_{II}$ and $\frac{1}{m_I} \nabla \psi_I \cdot \hat{n}_{I,II} = \frac{1}{m_{II}} \nabla \psi_{II} \cdot \hat{n}_{I,II}$, where $\hat{n}_{I,II}$ denotes the unit vector normal to the interface. Imposing the boundary conditions at the inner and outer radii of the core-shell quantum dot, the scattering coefficients can be found. In particular, $R_{l,1} = \mathbb{R}_{l,1}$, where

$$\mathbb{R}_{l,\alpha} = \frac{-q_{s,\alpha} m_h j_l(kb_\alpha) [j'_l(q_{s,\alpha} b_\alpha) + y'_l(q_{s,\alpha} b_\alpha) U_{l,\alpha}] + km_{s,\alpha} j'_l(kb_\alpha) [j_l(q_{s,\alpha} b_\alpha) + y_l(q_{s,\alpha} b_\alpha) U_{l,\alpha}]}{q_{s,\alpha} m_h h_l^{(1)}(kb_\alpha) [j'_l(q_{s,\alpha} b_\alpha) + y'_l(q_{s,\alpha} b_\alpha) U_{l,\alpha}] - km_{s,\alpha} h_l^{(1)}(kb_\alpha) [j_l(q_{s,\alpha} b_\alpha) + y_l(q_{s,\alpha} b_\alpha) U_{l,\alpha}]}\quad (4)$$

and

$$U_{l,\alpha} = -\frac{q_{c,\alpha} m_{s,\alpha} j_l(q_{s,\alpha} a_\alpha) j'_l(q_{c,\alpha} a_\alpha) - q_{s,\alpha} m_{c,\alpha} j'_l(q_{s,\alpha} a_\alpha) j_l(q_{c,\alpha} a_\alpha)}{q_{c,\alpha} m_{s,\alpha} y_l(q_{s,\alpha} a_\alpha) j'_l(q_{c,\alpha} a_\alpha) - q_{s,\alpha} m_{c,\alpha} y'_l(q_{s,\alpha} a_\alpha) j_l(q_{c,\alpha} a_\alpha)}.\quad (5)$$

The *far-zone* radial component of the scattered current is

$$\begin{aligned}j_r^{\text{sca}} &= \mathbf{j}^{\text{sca}} \cdot \hat{\mathbf{r}} = \frac{\hbar}{m_h} \text{Im}[\psi_{\text{sca}}^* \nabla \psi_{\text{sca}}] \cdot \hat{\mathbf{r}} \\ &\sim \frac{\hbar k}{m_h} \frac{b_1^2}{r^2} F_{\text{sca}}(\theta),\end{aligned}\quad (6)$$

where

$$\begin{aligned}F_{\text{sca}}(\theta) &= \frac{4\pi}{k^2 b_1^2} \text{Im} \left[i \sum_{l,l'} \sqrt{(2l+1)(2l'+1)} \right. \\ &\quad \left. \times R_{l,1}^* R_{l',1} Y_{l0}^*(\hat{\mathbf{r}}) Y_{l'0}(\hat{\mathbf{r}}) \right]\end{aligned}\quad (7)$$

characterizes the angular scattering of the quantum dot.

Now, we derive conditions for the nearly complete suppression of backward, forward, and both backward and forward scattering. In the case of dominant s and p waves,

$$F_{\text{sca}}(\theta) \propto |R_{0,1}|^2 + 6\text{Re}(R_{0,1}^* R_{1,1}) \cos \theta + 9|R_{1,1}|^2 \cos^2 \theta,\quad (8)$$

to a good approximation. Thus the scattering is directed mainly in the forward (backward) direction when $\text{Re}(R_{0,1}^* R_{1,1})$ is positive (negative). It follows that

$$\begin{aligned}R_{0,1} &= +3R_{1,1}, \\ R_{0,1} &= -3R_{1,1}\end{aligned}\quad (9)$$

almost ensure the suppression of backward scattering and forward scattering, respectively. Note that both $R_{0,1}$ and $R_{1,1}$ are complex numbers.

In the case of dominant p and d waves,

$$\begin{aligned}F_{\text{sca}}(\theta) &\propto 9|R_{1,1}|^2 \cos^2 \theta + \frac{25}{4} |R_{2,1}|^2 (3 \cos^2 \theta - 1)^2 \\ &\quad + 15 \text{Re}(R_{1,1}^* R_{2,1}) (3 \cos^2 \theta - 1) \cos \theta.\end{aligned}\quad (10)$$

Here

$$\begin{aligned}R_{1,1} &= +\frac{5}{3} R_{2,1}, \\ R_{1,1} &= -\frac{5}{3} R_{2,1}\end{aligned}\quad (11)$$

almost ensure the suppression of backward scattering and forward scattering, respectively.

The case of dominant s and d waves is far more interesting, since

$$\begin{aligned}F_{\text{sca}}(\theta) &\propto |R_{0,1}|^2 + \frac{25}{4} |R_{2,1}|^2 (3 \cos^2 \theta - 1)^2 \\ &\quad + 5 \text{Re}(R_{0,1}^* R_{2,1}) (3 \cos^2 \theta - 1)\end{aligned}\quad (12)$$

is a function of $\cos^2 \theta$ rather than $\cos \theta$. It follows that

$$R_{0,1} = -5R_{2,1}\quad (13)$$

almost ensures the simultaneous suppression of both forward and backward scattering.

Figure 2(a) shows the nearly complete suppression of backward scattering by a core-shell quantum dot. Here $m_h = 0.1m_e$, $m_{c,1} = 0.9m_e$, and $m_{s,1} = 2.2m_e$, where m_e denotes the mass of the electron. $a_1 = 1.5$ nm. In the case of dominant s and p waves, $R_{0,1} = 2.66e^{0.03\pi i} R_{1,1}$ when $b_1 = 2$ nm, $E = 58$, $V_{c,1} = -305$, and $V_{s,1} = -85$ meV. In the case of dominant p and d waves, $R_{1,1} = 1.45e^{0.01\pi i} R_{2,1}$ when $b_1 = 2$ nm, $E = 288$, $V_{c,1} = -80$, and $V_{s,1} = 95$ meV. Figure 2(b) shows the nearly complete suppression of forward scattering. Here s and p waves are dominant and $R_{0,1} = 3.3e^{0.97\pi i} R_{1,1}$ when $b_1 = 2$ nm, $E = 25$, $V_{c,1} = -80$, and $V_{s,1} = -60$ meV.

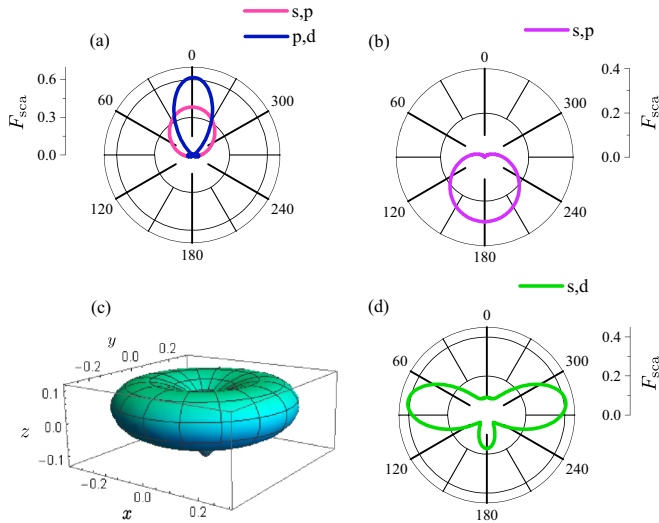


FIG. 2. $F_{\text{sca}}(\theta)$ of a core-shell quantum dot exhibiting (a) forward scattering due to s and p waves (pink line) or p and d waves (blue line), (b) backward scattering due to s and p waves, (c) and (d) transverse scattering due to s and d waves. The parameters are in the text.

The interesting case of transverse Kerker scattering due to the interference of s and d waves is shown in Figs. 2(c) and 2(d). Here $R_{0,1} = 4e^{0.82\pi i}R_{2,1}$ when $b_1 = 1.75$ nm, $E = 300$, $V_{c,1} = 70$, and $V_{s,1} = -25$ meV.

To design high-performance thermoelectric materials, inclusions are expected to exhibit directional forward scattering in a *broad* energy window. Such inclusions are not out of reach. For the quantum dot exemplified in Fig. 2(a), the ratio of forward to backward scattering is 10 644 and 439 at energies $E = 10$ and 58 meV, respectively, when $V_{c,1} = -305$ and $V_{s,1} = -85$ meV. More importantly, this ratio is greater than 1 in the whole energy window $E < 83$ meV.

Concerning the similarities between wave optics and wave mechanics, a few remarks are in order. (i) To study the electromagnetic wave scattering from a nanoparticle, the vector multipole fields—solutions of the Maxwell equations that are simultaneous eigenvectors of L^2 and L_z —are of use [41,51]: $\mathbf{J}_{lm}^{(1)}(\mathbf{r}, k) = j_l(kr)\mathbf{X}_{lm}(\hat{\mathbf{r}})$, $\mathbf{J}_{lm}^{(2)}(\mathbf{r}, k) = \frac{1}{k}\nabla \times \mathbf{J}_{lm}^{(1)}(\mathbf{r}, k)$, $\mathbf{H}_{lm}^{(1)}(\mathbf{r}, k) = h_l^{(1)}(kr)\mathbf{X}_{lm}(\hat{\mathbf{r}})$, and $\mathbf{H}_{lm}^{(2)}(\mathbf{r}, k) = \frac{1}{k}\nabla \times \mathbf{H}_{lm}^{(1)}(\mathbf{r}, k)$, where $\mathbf{X}_{lm} = [l(l+1)]^{-1/2}\mathbf{L}Y_{lm}$ are vector spherical harmonics. \mathbf{H} -multipole fields satisfy the radiation condition at infinity. To study the matter wave scattering from a quantum dot, we expand the wave functions in terms of $j_l(kr)Y_{lm}(\hat{\mathbf{r}})$ and $h_l^{(1)}(kr)Y_{lm}(\hat{\mathbf{r}})$, which satisfy the boundary condition at infinity. The spherical harmonics $Y_{lm}(\hat{\mathbf{r}})$ are simultaneous eigenfunctions of L^2 and L_z . (ii) The Maxwell and Schrödinger wave equations are different in many respects. In other words, there is no one-to-one correspondence between the worlds of electromagnetic and matter waves. For example, an *electric* multipole field is distinct from a *magnetic* one labeled by the same angular momentum numbers. But a partial matter wave is labeled only by the angular momentum numbers. (iii) Identically zero forward scattering of electromagnetic waves from a magnetodielectric nanoparticle is forbidden by the optical theorem [52]. In a similar vein, the optical

theorem implies the *nearly complete* rather than the complete suppression of forward scattering of matter waves from a quantum dot.

IV. ELECTRON SCATTERING FROM A CLUSTER OF QUANTUM DOTS

We consider electron wave scattering from an aggregate of core-shell quantum dots. A point P of position $\mathbf{r} = (r \sin \theta \cos \phi, r \sin \theta \sin \phi, r \cos \theta)$ has position $\mathbf{r}_\alpha = r_\alpha \hat{\mathbf{r}}_\alpha = \mathbf{r} - \mathbf{d}_\alpha$ in the frame of reference centered at O_α . In this frame, the incident wave can be expanded as

$$\begin{aligned} \psi_{\text{inc}} &= e^{i\mathbf{k}\cdot\mathbf{r}} = e^{i\mathbf{k}\cdot(\mathbf{r}_\alpha + \mathbf{d}_\alpha)} \\ &= e^{i\mathbf{k}\cdot\mathbf{d}_\alpha} \sum_{l=0}^{\infty} i^l \sqrt{4\pi(2l+1)} j_l(kr_\alpha) Y_{l0}(\hat{\mathbf{r}}_\alpha). \end{aligned} \quad (14)$$

The transmitted and scattered waves can be expanded as well:

$$\begin{aligned} \psi_{\text{core},\alpha} &= \sum_{l=0}^{\infty} i^l \sqrt{4\pi(2l+1)} T_{l,\alpha}^c j_l(q_{c,\alpha} r_\alpha) Y_{l0}(\hat{\mathbf{r}}_\alpha), \\ \psi_{\text{shell},\alpha} &= \sum_{l=0}^{\infty} i^l \sqrt{4\pi(2l+1)} [T_{l,\alpha}^s j_l(q_{s,\alpha} r_\alpha) \\ &\quad + T_{l,\alpha}^{s'} y_l(q_{s,\alpha} r_\alpha)] Y_{l0}(\hat{\mathbf{r}}_\alpha), \\ \psi_{\text{sca}} &= \sum_l i^l \sqrt{4\pi(2l+1)} [R_{l,\alpha} h_l^{(1)}(kr_\alpha) Y_{l0}(\hat{\mathbf{r}}_\alpha) \\ &\quad + \sum_{\alpha' \neq \alpha} R_{l,\alpha'} h_l^{(1)}(kr_{\alpha'}) Y_{l0}(\hat{\mathbf{r}}_{\alpha'})]. \end{aligned} \quad (15)$$

The scattered wave is naturally expressed as the superposition of waves scattered by all the quantum dots. Employing the Nozawa's addition theorem (see Appendix A) to write the scattered wave in terms of eigenfunctions centered at O_α , and imposing the boundary conditions at the inner and outer radii of the α th core-shell quantum dot, we find a set of linear equations for the scattering coefficients (see Appendix B). Eliminating the coefficients $T_{l,\alpha}^c$, $T_{l,\alpha}^s$, and $T_{l,\alpha}^{s'}$ from these equations, we find that

$$\begin{aligned} R_{l,\alpha} &= \sum_{\alpha' \neq \alpha} \sum_{l'=0}^{\infty} i^{l'-l} \sqrt{\frac{2l'+1}{2l+1}} \mathbb{R}_{l,\alpha} G_{l0,l'0}(\mathbf{d}_{\alpha'\alpha}, k) R_{l',\alpha'} \\ &\quad + \mathbb{R}_{l,\alpha} e^{i\mathbf{k}\cdot\mathbf{d}_\alpha}, \end{aligned} \quad (16)$$

where $\mathbb{R}_{l,\alpha}$ describe the scattering from *one isolated* quantum dot [see Eq. (4)]. The above equation can be written in a more compact matrix form $\mathbf{R}_{\text{cluster}} = \mathbf{R}_{\text{dot}} + \mathbf{M}\mathbf{R}_{\text{cluster}}$, whose solution is

$$\mathbf{R}_{\text{cluster}} = (\mathbf{I} - \mathbf{M})^{-1} \mathbf{R}_{\text{dot}}. \quad (17)$$

Here

$$\begin{aligned} \mathbf{R}_{\text{cluster}} &= [(R_{0,1}, \dots, R_{l,1}), \dots, (R_{0,N}, \dots, R_{l,N})]^T, \\ \mathbf{R}_{\text{dot}} &= [e^{ik \cdot d_1} (\mathbb{R}_{0,1}, \dots, \mathbb{R}_{l,1}), \dots, \\ &\quad \times e^{ik \cdot d_N} (\mathbb{R}_{0,N}, \dots, \mathbb{R}_{l,N})]^T, \\ \mathbf{M}_{l\alpha, l'\alpha'} &= i^{l'-l} \sqrt{\frac{2l'+1}{2l+1}} \mathbb{R}_{l,\alpha} G_{l0, l'0}(\mathbf{d}_{\alpha'\alpha}, k) (1 - \delta_{\alpha\alpha'}). \end{aligned} \quad (18)$$

We again employ the Nozawa's addition theorem to rewrite ψ_{sca} in terms of wave functions centered at the origin

$$\psi_{\text{sca}} = \sum_{lm} i^{l'-l} \sqrt{4\pi(2l+1)} \mathcal{R}_{lm} h_l^{(1)}(kr) Y_{lm}(\hat{\mathbf{r}}). \quad (19)$$

Here $r > d_\alpha$ and

$$\mathcal{R}_{lm} = \sum_{\alpha=1}^N \sum_{l'=0}^{\infty} i^{l'-l} \sqrt{\frac{2l'+1}{2l+1}} G_{lm, l'0}(-\mathbf{d}_\alpha, k) \mathbf{R}_{l', \alpha} \quad (20)$$

is the effective scattering coefficient of the cluster. In general, the scattered wave ψ_{sca} depends on the azimuthal angle ϕ , since the cluster is not rotationally symmetric about the $\hat{\mathbf{z}}$ axis. Moreover, the s , p , d , and even f wave contribution to the scattered wave may be significant. Now it is straightforward to calculate the *far-zone* radial component of the scattered current,

$$\begin{aligned} j_r^{\text{sca}} &= \mathbf{j}^{\text{sca}} \cdot \hat{\mathbf{r}} = \frac{\hbar}{m_h} \text{Im}[\psi_{\text{sca}}^* \nabla \psi_{\text{sca}}] \cdot \hat{\mathbf{r}} \\ &\sim \frac{\hbar k}{m_h} \frac{\bar{b}^2}{r^2} F_{\text{sca}}(\hat{\mathbf{r}}), \end{aligned} \quad (21)$$

where

$$\begin{aligned} F_{\text{sca}}(\hat{\mathbf{r}}) &= \frac{4\pi}{k^2 \bar{b}^2} \text{Im} \left[i \sum_{lm'l'm'} \sqrt{(2l+1)(2l'+1)} \mathcal{R}_{lm}^* \right. \\ &\quad \left. \times \mathcal{R}_{l'm'} Y_{lm}^*(\hat{\mathbf{r}}) Y_{l'm'}(\hat{\mathbf{r}}) \right] \end{aligned} \quad (22)$$

characterizes the angular scattering of the cluster. In particular $F_{\text{sca}}(\theta = 0, \phi)$, $F_{\text{sca}}(\theta = 180^\circ, \phi)$, and $F_{\text{sca}}(\theta = 0, \phi)/F_{\text{sca}}(\theta = 180^\circ, \phi)$ characterize forward scattering (F), backward scattering (B), and the ratio of forward to backward scattering (F/B), respectively. The incident current is $\mathbf{j}^{\text{inc}} = \frac{\hbar k}{m_h} \hat{\mathbf{z}}$. Moreover, the total geometrical cross section of quantum dots is $\sum_{\alpha=1}^N \pi b_\alpha^2 = N\pi \bar{b}^2$. Thus it is appropriate to adopt

$$\begin{aligned} Q_N^{\text{sca}} &= \frac{\int j_r^{\text{sca}} r^2 d\Omega}{j^{\text{inc}} N\pi \bar{b}^2} \\ &= \frac{4}{Nk^2 \bar{b}^2} \sum_{lm} (2l+1) |\mathcal{R}_{lm}|^2, \end{aligned} \quad (23)$$

as the scattering efficiency of the cluster.

In the following numerical examples devoted to the multiple scattering phenomena, we consider identical quantum dots with $m_{c,\alpha} = 0.9m_e$ and $m_{s,\alpha} = 2.2m_e$, $a_\alpha = 1.5$ and $b_\alpha = 2$ nm. We fix $V_{c,\alpha} = -30$ meV but adjust $V_{s,\alpha}$.

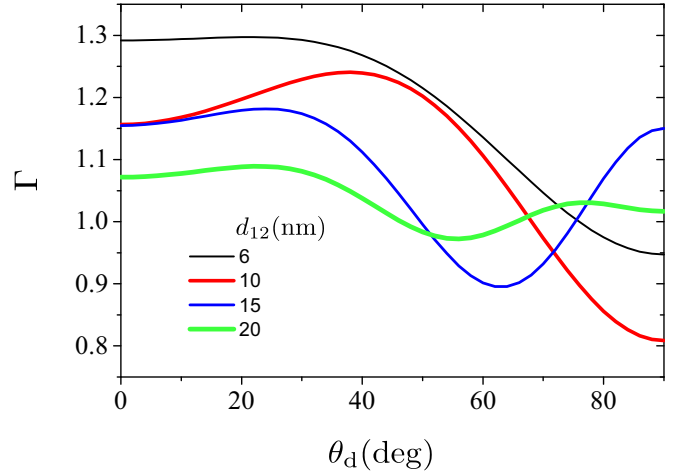


FIG. 3. Γ of a dimer of core-only quantum dots, as a function of θ_d for various d_{12} . Here $m_h = 0.7m_e$ and $E = 10$ meV. $\Gamma < 1$ represents the shadow effect in electron scattering.

A. The shadow effect

The so-called shadow effect is known in the realm of electromagnetic wave scattering from dielectric spheres [41]. As an interesting consequence of multiple scattering, the scattering cross section of a cluster of dielectric spheres may be *less* than the sum of the scattering cross sections of the constituent spheres considered as independent scatterers.

Here we demonstrate the shadow effect in the realm of electron wave scattering from quantum dots. We consider a dimer composed of two identical core-only quantum dots positioned at $-\frac{1}{2}d_{12}(\sin \theta_d, 0, \cos \theta_d)$ and $+\frac{1}{2}d_{12}(\sin \theta_d, 0, \cos \theta_d)$. Indeed d_{12} is the dimer length, and θ_d is the angle between the dimer axis and the incident electron wave vector. We assume that $m_h = 0.7m_e$ and $E = 10$ meV. We focus on

$$\Gamma = \frac{Q_2^{\text{sca}}}{Q_1^{\text{sca}}}, \quad (24)$$

where Q_2^{sca} and Q_1^{sca} denote the scattering efficiencies of a dimer and a single quantum dot, respectively. Figure 3 demonstrates that Γ may become less than 1.

B. Kerker scattering of electrons: Ultradirectional forward scattering

In view of applications in nanoantennas, nanolasers, and photovoltaics, ultradirectional light scattering has gained interest. It is demonstrated that the directionality of the forward scattering can be significantly increased upon the excitation of electric and magnetic multipoles rather than the electric and magnetic dipoles. Furthermore, significant suppression of undesired side lobes and enhancement of unidirectional scattering can be achieved by arranging the nanoparticles in a *chain* [53–57]. Indeed multiple scattering effects are of great importance in clusters: The electric and magnetic multipoles induced in each nanoparticle of the cluster are different from those induced in an isolated nanoparticle. Here we focus on the ultradirectional electron scattering by a cluster of quantum dots in view of futuristic thermoelectric materials.

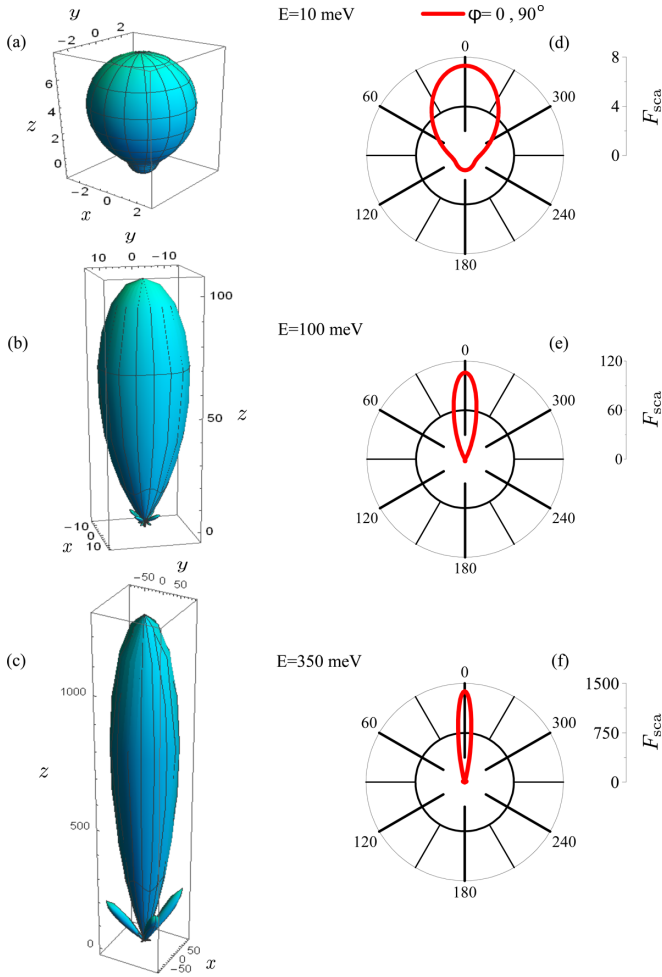


FIG. 4. $F_{\text{sca}}(\theta, \phi)$ of a symmetric quadrumer of core-only quantum dots for (a) $E = 10$ meV, (b) $E = 100$ meV, and (c) $E = 350$ meV. Corresponding plots of $F_{\text{sca}}(\theta, \phi = 0, 90^\circ)$ are in panels (d)–(f). Here $m_h = 0.7m_e$.

We consider a *symmetric* quadrumer composed of four *core-only* quantum dots at $(3,0,0)$, $(-3,0,0)$, $(0,3,0)$, and $(0,-3,0)$ nm. The plane of the cluster is perpendicular to the \hat{z} axis, the propagation direction of the incident wave. We assume that $m_h = 0.7m_e$. Figure 4 shows $F_{\text{sca}}(\theta, \phi)$ of this symmetric quadrumer for $E = 10$, 100, and 350 meV. Here the scattering pattern has fourfold rotational symmetry about the \hat{z} axis. Moreover, the scattering pattern is highly pronounced in the forward direction. To better characterize the directionality of the scattering, we use the main lobe angular width θ_{FWHM} defined as the full width at half maximum of $F_{\text{sca}}(\theta, \phi = 0)$. At these three energies, θ_{FWHM} is 45° , 15° , and 8° , the maximum of the main lobe 7.3, 107, and 1400 is quite considerable, and the side lobe is smaller by a factor 6, 158, and 215, respectively. At these three energies, the ultradirectional forward scattering originates from the interference of partial waves with angular momenta $l \leq 4$, 8, and 14, respectively. In other words, to realize ultradirectional forward scattering, the excitation of high angular momentum partial waves is of importance.

C. Kerker scattering of electrons: Suppression of forward scattering

Many theoretical and experimental studies are devoted to superbackscattering of electromagnetic waves [13,14,58–60]. Notably, it has been recognized that enhanced backscattering may pave the way toward *negative* scattering asymmetry parameter g (defined as the average of the cosine of the scattering angle) [61,62]. To describe diffusive light transport in random particulate media, the scattering mean free path ℓ_s and the transport mean free path $\ell^* = \ell_s/(1 - g)$ are of importance. An unusual negative g makes ℓ^* *less* than ℓ_s . In respect of the Anderson localization, this unusual multiple scattering regime deserves attention. Here we focus on the suppression of forward electron scattering by a cluster of quantum dots.

We consider a dimer composed of two quantum dots at $(3,0,0)$ and $(-3,0,0)$ nm. We assume that $m_h = 0.1m_e$. Figure 5(a1) shows that for all incident electron energies $E < 90$ meV, the core-only dimer has a very strong forward scattering. Particularly around $E = 10$ meV one finds that $F/B > 2300$. Using core-shell rather than core-only quantum dots allows engineering the angular scattering pattern. Figure 5(a2) shows dramatic suppression of forward scattering; indeed one finds that in general $F/B < 100$, and in particular $0.01 < F/B < 1$ when $42 < E < 85$ meV. Here $V_{s,\alpha} = -260$ meV. Figure 5(a3) better demonstrates the Kerker scattering of electrons. Here $E = 88$ and $V_{s,\alpha} = -260$ meV are assumed. $F_{\text{sca}}(\theta, \phi = 0)$ of a core-only dimer (red line) is pronounced in the forward region $\theta < 35^\circ$ and is maximum when $\theta = 0$. Nevertheless, $F_{\text{sca}}(\theta, \phi = 0)$ of a core-shell dimer (blue line) is pronounced in the backward region $155^\circ < \theta$ and is maximum when $\theta = 180^\circ$. Figure 5(a4) conveys the same message. Here $E = 10$ and $V_{s,\alpha} = 110$ meV. The angular scattering pattern of more complicated clusters can be engineered as well. Figures 5(b1)–5(b4) confirm Kerker scattering of electrons from an *asymmetric* quadrumer composed of four quantum dots at $(5,0,0)$, $(-5,0,0)$, $(-6,-6,-6)$, and $(7,7,0)$ nm.

The left and right panels of Fig. 6 vividly demonstrate the contribution of partial waves to the scattering pattern of the core-only and core-shell dimer, respectively. Note the different scales of rows. Here a double such as (s, p) or a triple such as (s, p, d) denotes the contribution of all terms with angular momenta 0 and 1, and all terms with angular momenta 0, 1, and 2 to the scattering pattern, respectively [see Eq. (22)]. Now it is clear that the strong suppression of forward scattering is a consequence of the interference of high angular momentum partial waves.

D. Transverse Kerker scattering of electrons

As mentioned before, the transverse Kerker scattering of light due to the interference of four multipoles (electric and magnetic dipoles, and electric and magnetic quadrupoles) is demonstrated [19]. Here we focus on the transverse Kerker scattering of electrons by a cluster of quantum dots in view of futuristic thermoelectric materials.

We consider a trimer composed of three core-only quantum dots at $(0,0,3)$, $(0,0,-3)$, and $(3,0,0)$ nm, and a quadrumer composed of four core-only quantum dots at $(0,0,3)$, $(0,0,-3)$, $(0,3,0)$, and $(0,-3,0)$ nm. We assume that

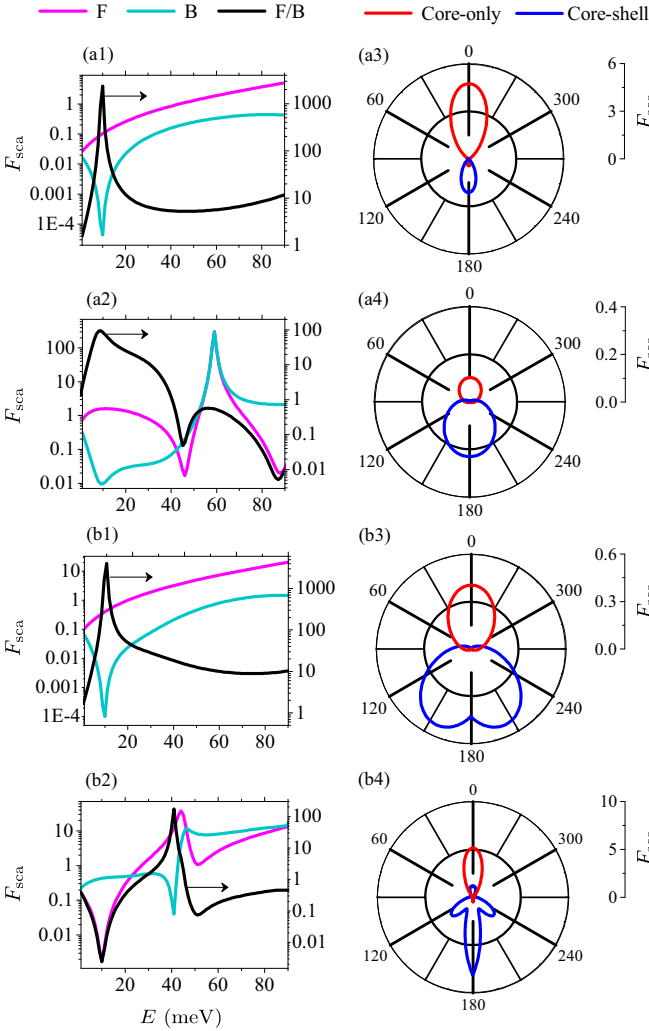


FIG. 5. $F_{\text{sca}}(\theta = 0, \phi)$, $F_{\text{sca}}(\theta = 180^\circ, \phi)$, and $F_{\text{sca}}(\theta = 0, \phi)/F_{\text{sca}}(\theta = 180^\circ, \phi)$ as a function of E for (a1) core-only dimer and (a2) core-shell dimer when $V_{s,\alpha} = -260$ meV. $F_{\text{sca}}(\theta, \phi = 0)$ of a core-only dimer (red line) and of a core-shell dimer (blue line) when (a3) $E = 88$ and $V_{s,\alpha} = -260$ meV and (a4) $E = 10$ and $V_{s,\alpha} = 110$ meV. Similar plots for an asymmetric quadrumer are in panels (b1)–(b4). Here $V_{s,\alpha} = 105$ meV. $E = 10$ and 51 meV in panels (b3) and (b4), respectively. In all plots $m_h = 0.1m_e$.

$m_h = 0.1m_e$ and $V_{c,\alpha} = 250$ meV. Figure 7 vividly illustrates transverse Kerker scattering of electrons by this trimer and quadrumer, for $E = 50$ and 65 meV, respectively. Indeed the interference of s , p , and d (s , d , and f) waves results in the peculiar scattering pattern of the trimer (quadrumer).

V. CONCLUSION

In summary, we presented a generalized partial wave method to treat the electron multiple scattering by a cluster of spherical core-shell quantum dots embedded in a host semiconductor. Guided by the multiparticle Mie theory, we expanded the incident, scattered, and transmitted wave functions in terms of the simultaneous eigenfunctions of the Hamiltonian of the pristine semiconductor and angular momentum operator. We used the Nozawa's addition theorem to

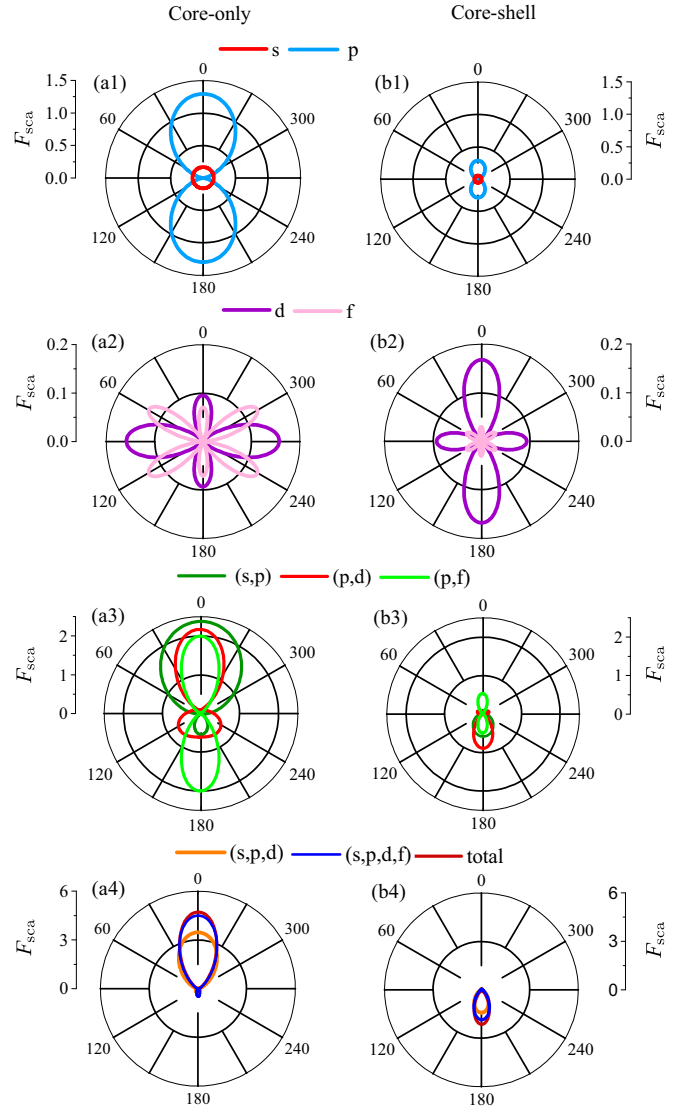


FIG. 6. Contribution of various partial waves to the scattering pattern of the core-only dimer. (a1) s and p , (a2) d and f , (a3) (s, p) , (p, d) , and (p, f) , (a4) (s, p, d) , (s, p, d, f) , and all partial waves. Right panels (b1)–(b4) pertain to the core-shell dimer. Here $m_h = 0.1m_e$, $E = 88$, and $V_{s,\alpha} = -260$ meV.

relate the expansion of the scattered and transmitted waves to that of the incident wave via imposing the boundary conditions at the inner and outer radii of all core-shell quantum dots. This naturally considers the electron multiple scattering from quantum dots. Inspired by the multipolar interference effects in nanophotonics, we theoretically demonstrated Kerker scattering and transverse Kerker scattering of matter waves by one or a cluster of spherical core-shell quantum dots.

Our results may open exciting opportunities for the development of new thermoelectric materials. To provide a high concentration of electrons, thermoelectrics are usually heavily doped with impurity atoms. But such traditional dopants considerably scatter the conduction electrons and consequently limit their mobility. To enhance the thermoelectric performance, untraditional dopants exhibiting ultradirectional forward scattering deserve attention: Such dopants are

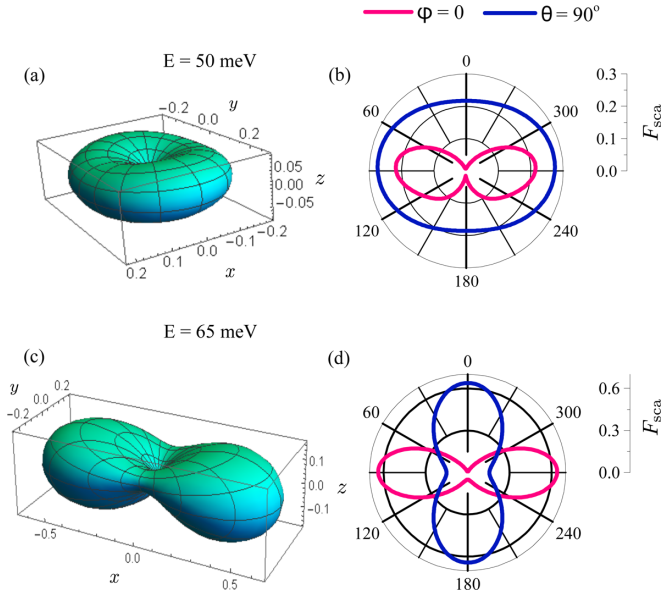


FIG. 7. (a) $F_{\text{sca}}(\theta, \phi)$ and (b) $F_{\text{sca}}(\theta, \phi = 0)$ and $F_{\text{sca}}(\theta = 90^\circ, \phi)$ of a trimer of core-only quantum dots, when $m_h = 0.1m_e$, $E = 50$, and $V_{c,\alpha} = 250$ meV. Similar plots for a quadrumer of core-only quantum dots when $E = 65$ meV are in panels (c) and (d), respectively.

almost unseeable to the electrons. We showed that core-shell quantum dot clusters may serve as phonon-blocking/electron-transmitting inclusions. Indeed experiments have already confirmed that thermoelectric properties of bulk

semiconductors can be improved by incorporation of nanoparticles [46–49]. We believe that the addition of designed core-shell rather than core-only quantum dots into the host matrix is not out of reach. Thus “Kerker scatterers” may pave the way towards futuristic thermoelectric materials.

APPENDIX A: NOZAWA’S ADDITION THEOREM

The Nozawa’s addition theorem states that [41]

$$h_l^{(1)}(kr_{\alpha'})Y_{lm}(\hat{\mathbf{r}}_{\alpha'}) = \sum_{l'm'} \vartheta_{l'}(kr_{\alpha})Y_{l'm'}(\hat{\mathbf{r}}_{\alpha})G_{l'm',lm}(\mathbf{d}_{\alpha'\alpha}, k).$$

Here $\mathbf{d}_{\alpha'\alpha} = \mathbf{d}_{\alpha} - \mathbf{d}_{\alpha'}$ and $d_{\alpha'\alpha} = |\mathbf{d}_{\alpha'\alpha}|$. Moreover,

$$G_{l'm',lm}(\mathbf{d}_{\alpha'\alpha}, k) = 4\pi \sum_L i^{l'-l+L} I(lm, L, l'm') v_L(kd_{\alpha'\alpha}) \times Y_{L,m'-m}^*(\hat{\mathbf{d}}_{\alpha'\alpha}),$$

where $\vartheta_{l'} = j_{l'}$ and $v_L = h_L$ for $r_{\alpha} < d_{\alpha'\alpha}$, and $\vartheta_{l'} = h_{l'}$ and $v_L = j_L$ for $r_{\alpha} > d_{\alpha'\alpha}$. The Gaunt integral $I(lm, L, l'm') = \int Y_{lm} Y_{LM} Y_{l'm'}^* d\Omega$ can be conveniently expressed in terms of the Clebsch-Gordan coefficients.

APPENDIX B: THE SCATTERING COEFFICIENTS

The scattering coefficients can be found from the following set of linear equations:

$$j_l(q_{s,\alpha} a_{\alpha}) T_{l,\alpha}^s + y_l(q_{s,\alpha} a_{\alpha}) T_{l,\alpha}^{s'} = j_l(q_{c,\alpha} a_{\alpha}) T_{l,\alpha}^c,$$

$$\frac{q_{s,\alpha}}{m_{s,\alpha}} [j_l'(q_{s,\alpha} a_{\alpha}) T_{l,\alpha}^s + y_l'(q_{s,\alpha} a_{\alpha}) T_{l,\alpha}^{s'}] = \frac{q_{c,\alpha}}{m_{c,\alpha}} j_l'(q_{c,\alpha} a_{\alpha}) T_{l,\alpha}^c,$$

$$e^{ik \cdot \mathbf{d}_{\alpha}} j_l(kb_{\alpha}) + h_l^{(1)}(kb_{\alpha}) R_{l,\alpha} + \sum_{\alpha' \neq \alpha, l'} i^{l'-l} \sqrt{\frac{2l'+1}{2l+1}} j_l(kb_{\alpha}) G_{l0,l'0}(\mathbf{d}_{\alpha'\alpha}, k) R_{l',\alpha'} = j_l(q_{s,\alpha} b_{\alpha}) T_{l,\alpha}^s + y_l(q_{s,\alpha} b_{\alpha}) T_{l,\alpha}^{s'},$$

$$\frac{k}{m_h} \left[e^{ik \cdot \mathbf{d}_{\alpha}} j_l'(kb_{\alpha}) + h_l^{(1)'}(kb_{\alpha}) R_{l,\alpha} + \sum_{\alpha' \neq \alpha, l'} i^{l'-l} \sqrt{\frac{2l'+1}{2l+1}} j_l'(kb_{\alpha}) G_{l0,l'0}(\mathbf{d}_{\alpha'\alpha}, k) R_{l',\alpha'} \right]$$

$$= \frac{q_{s,\alpha}}{m_{s,\alpha}} [j_l'(q_{s,\alpha} b_{\alpha}) T_{l,\alpha}^s + y_l'(q_{s,\alpha} b_{\alpha}) T_{l,\alpha}^{s'}].$$

- [1] S. V. Gaponenko, *Introduction to Nanophotonics* (Cambridge University Press, Cambridge, 2010).
- [2] L. Novotny and B. Hecht, *Principles of Nano-Optics* (Cambridge University Press, New York, 2012).
- [3] K. Li, M. I. Stockman, and D. J. Bergman, Self-Similar Chain of Metal Nanospheres as an Efficient Nanolens, *Phys. Rev. Lett.* **91**, 227402 (2003).
- [4] M. L. Brongersma, J. W. Hartman, and H. A. Atwater, Electromagnetic energy transfer and switching in nanoparticle chain arrays below the diffraction limit, *Phys. Rev. B* **62**, R16356 (2000).
- [5] S. A. Maier, P. G. Kik, H. A. Atwater, S. Meltzer, E. Harel, B. E. Koel, and A. A. G. Requicha, Local detection of electromagnetic energy transport below the diffraction limit in metal nanoparticle plasmon waveguides, *Nat. Mater.* **2**, 229 (2003).

- [6] L. Novotny and N. van Hulst, Antennas for light, *Nat. Photonics* **5**, 83 (2011).
- [7] M. Kerker, D.-S. Wang, and C. L. Giles, Electromagnetic scattering by magnetic spheres, *J. Opt. Soc. Am.* **73**, 765 (1983).
- [8] W. Cai and V. Shalaev, *Optical Metamaterials: Fundamentals and Applications* (Springer, New York, 2010).
- [9] C. Simovski and S. Tretyakov, *An Introduction to Metamaterials and Nanophotonics* (Cambridge University Press, Cambridge, 2020).
- [10] A. I. Kuznetsov, A. E. Miroschnichenko, Y. H. Fu, J. Zhang, and B. Luk'yanchuk, Magnetic light, *Sci. Rep.* **2**, 492 (2012).
- [11] A. B. Evlyukhin, S. M. Novikov, U. Zywietz, R. L. Eriksen, C. Reinhardt, S. I. Bozhevolnyi, and B. N. Chichkov, Demonstration of magnetic dipole resonances of dielectric nanospheres in the visible region, *Nano Lett.* **12**, 3749 (2012).

- [12] D. Permyakov, I. Sinev, D. Markovich, P. Ginzburg, A. Samusev, P. Belov, V. Valuckas, A. I. Kuznetsov, B. S. Luk'yanchuk, A. E. Miroshnichenko, D. N. Neshev, and Y. S. Kivshar, Probing magnetic and electric optical responses of silicon nanoparticles, *Appl. Phys. Lett.* **106**, 171110 (2015).
- [13] J. M. Geffrin, B. García-Cámara, R. Gómez-Medina, P. Albella, L. S. Froufe-Pérez, C. Eyraud, A. Litman, R. Vaillon, F. González, M. Nieto-Vesperinas, J. J. Sáenz, and F. Moreno, Magnetic and electric coherence in forward- and back-scattered electromagnetic waves by a single dielectric subwavelength sphere, *Nat. Commun.* **3**, 1171 (2012).
- [14] Y. H. Fu, A. I. Kuznetsov, A. E. Miroshnichenko, Y. F. Yu, and B. Luk'yanchuk, Directional visible light scattering by silicon nanoparticles, *Nat. Commun.* **4**, 1527 (2013).
- [15] W. Liu and Y. S. Kivshar, Multipolar interference effects in nanophotonics, *Philos. Trans. R. Soc. A* **375**, 20160317 (2017).
- [16] W. Liu and Y. S. Kivshar, Generalized Kerker effects in nanophotonics and meta-optics, *Opt. Express* **26**, 13085 (2018).
- [17] J. Y. Lee, A. E. Miroshnichenko, and R.-K. Lee, Simultaneously nearly zero forward and nearly zero backward scattering objects, *Opt. Express* **26**, 30393 (2018).
- [18] A. Bag, M. Neugebauer, P. Woźniak, G. Leuchs, and P. Banzer, Transverse Kerker Scattering for Angstrom Localization of Nanoparticles, *Phys. Rev. Lett.* **121**, 193902 (2018).
- [19] H. K. Shamkhi, K. V. Baryshnikova, A. Sayanskiy, P. Kapitanova, P. D. Terekhov, P. Belov, A. Karabchevsky, A. B. Evlyukhin, Y. Kivshar, and A. S. Shalin, Transverse Scattering and Generalized Kerker Effects in All-Dielectric Mie-Resonant Metaoptics, *Phys. Rev. Lett.* **122**, 193905 (2019).
- [20] Y. Yu, J. Liu, Y. Yu, D. Qiao, Y. Li, and R. Salas-Montiel, Broadband unidirectional transverse light scattering in a V-shaped silicon nanoantenna, *Opt. Express* **30**, 7918 (2022).
- [21] M. M. Bukharin, V. Y. Pecherkin, A. K. Ospanova, V. B. Il'in, L. M. Vasilyak, A. A. Basharin, and B. Luk'yanchuk, Transverse Kerker effect in all-dielectric spheroidal particles, *Sci. Rep.* **12**, 7997 (2022).
- [22] F. Qin, Z. Zhang, K. Zheng, Y. Xu, S. Fu, Y. Wang, and Y. Qin, Transverse Kerker Effect for Dipole Sources, *Phys. Rev. Lett.* **128**, 193901 (2022).
- [23] J. H. Yan, P. Liu, Z. Y. Lin, H. Wang, H. J. Chen, C. X. Wang, and G. W. Yang, Magnetically induced forward scattering at visible wavelengths in silicon nanosphere oligomers, *Nat. Commun.* **6**, 7042 (2015).
- [24] J. van de Groep, J. van de Groep, T. Coenen, S. A. Mann, and A. Polman, Direct imaging of hybridized eigenmodes in coupled silicon nanoparticles, *Optica* **3**, 93 (2016).
- [25] Á. I. Barreda, H. Saleh, A. Litman, F. González, J.-M. Geffrin, and F. Moreno, Electromagnetic polarization-controlled perfect switching effect with high-refractive-index dimers and the beam-splitter configuration, *Nat. Commun.* **8**, 13910 (2017).
- [26] G. Lu, Y. Wang, R. Y. Chou, H. Shen, Y. He, Y. Cheng, and Q. Gong, Directional side scattering of light by a single plasmonic trimer, *Laser Photonics Rev.* **9**, 530 (2015).
- [27] P. Banzer, P. Woźniak, U. Mick, I. D. Leon, and R. W. Boyd, Chiral optical response of planar and symmetric nanotrimers enabled by heteromaterial selection, *Nat. Commun.* **7**, 13117 (2016).
- [28] H. K. Shamkhi, A. Sayanskiy, A. C. Valero, A. S. Kupriianov, P. Kapitanova, Y. S. Kivshar, A. S. Shalin, and V. R. Tuz, Transparency and perfect absorption of all-dielectric resonant metasurfaces governed by the transverse Kerker effect, *Phys. Rev. Materials* **3**, 085201 (2019).
- [29] D. Dragoman and M. Dragoman, *Quantum-Classical Analogies* (Springer, Berlin, 2004).
- [30] T. K. Gaylord and K. F. Brennan, Electron wave optics in semiconductors, *J. Appl. Phys.* **65**, 814 (1989).
- [31] Y. Ji, Y. Chung, D. Sprinzak, M. Heiblum, D. Mahalu, and H. Shtrikman, An electronic Mach-Zehnder interferometer, *Nature (London)* **422**, 415 (2003).
- [32] B. Liao, M. Zebarjadi, K. Esfarjani, and G. Chen, Cloaking Core-Shell Nanoparticles from Conducting Electrons in Solids, *Phys. Rev. Lett.* **109**, 126806 (2012).
- [33] M. Zebarjadi, B. Liao, K. Esfarjani, M. Dresselhaus, and G. Chen, Enhancing the thermoelectric power factor by using invisible dopants, *Adv. Mater.* **25**, 1577 (2013).
- [34] R. Fleury and A. Alù, Quantum cloaking based on scattering cancellation, *Phys. Rev. B* **87**, 045423 (2013).
- [35] J. Y. Lee and R.-K. Lee, Hiding the interior region of core-shell nanoparticles with quantum invisible cloaks, *Phys. Rev. B* **89**, 155425 (2014).
- [36] C. Valagiannopoulos, Perfect quantum cloaking of tilted cylindrical nanocavities, *Phys. Rev. B* **101**, 195301 (2020).
- [37] B. Liao, M. Zebarjadi, K. Esfarjani, and G. Chen, Isotropic and energy-selective electron cloaks on graphene, *Phys. Rev. B* **88**, 155432 (2013).
- [38] D. Oliver, J. H. Garcia, T. G. Rappoport, N. M. R. Peres, and F. A. Pinheiro, Cloaking resonant scatterers and tuning electron flow in graphene, *Phys. Rev. B* **91**, 155416 (2015).
- [39] M. Sadrara and M. F. Miri, Dirac electron scattering from a cluster of electrostatically defined quantum dots in graphene, *Phys. Rev. B* **99**, 155432 (2019).
- [40] M. Sadrara and M. F. Miri, Collective cloaking of a cluster of electrostatically defined core-shell quantum dots in graphene, *J. Phys.: Condens. Matter* **34**, 115703 (2022).
- [41] F. Borghese, P. Denti, and R. Saija, *Scattering from Model Nonspherical Particles* (Springer, Berlin, 2007).
- [42] C. Forman, I. K. Muritala, R. Pardemann, and B. Meyer, Estimating the global waste heat potential, *Renewable Sustainable Energy Rev.* **57**, 1568 (2016).
- [43] L. E. Bell, Cooling, heating, generating power, and recovering waste heat with thermoelectric systems, *Science* **321**, 1457 (2008).
- [44] D. Li, Y. Gong, Y. Chen, J. Lin, Q. Khan, Y. Zhang, Y. Li, H. Zhang, and H. Xie, Recent progress of two-dimensional thermoelectric materials, *Nano-Micro Lett.* **12**, 36 (2020).
- [45] S. Zhao, B. Dong, H. Wang, H. Wang, Y. Zhang, Z. V. Han, and H. Zhang, In-plane anisotropic electronics based on low-symmetry 2D materials: Progress and prospects, *Nanoscale Adv.* **2**, 109 (2020).
- [46] J. P. Heremans, C. M. Thrush, and D. T. Morelli, Thermopower enhancement in lead telluride nanostructures, *Phys. Rev. B* **70**, 115334 (2004).
- [47] K. F. Hsu, S. Loo, F. Guo, W. Chen, J. S. Dyck, C. Uher, T. Hogan, E. K. Polychroniadis, and M. G. Kanatzidis, Cubic $\text{AgPb}_m\text{SbTe}_{2+m}$: Bulk thermoelectric materials with high figure of merit, *Science* **303**, 818 (2004).
- [48] J. P. Heremans, C. M. Thrush, and D. T. Morelli, Thermopower enhancement in PbTe with Pb precipitates, *J. Appl. Phys.* **98**, 063703 (2005).

- [49] M. Zebarjadi, K. Esfarjani, A. Shakouri, Z. X. Bian, J. H. Bahk, G. H. Zeng, J. Bowers, H. Lu, J. Zide, and A. Gossard, Effect of nanoparticles on electron and thermoelectric transport, *J. Electron. Mater.* **38**, 954 (2009).
- [50] M. Zebarjadi, K. Esfarjani, Z. Bian, and A. Shakouri, Low-temperature thermoelectric power factor enhancement by controlling nanoparticle size distribution, *Nano Lett.* **11**, 225 (2011).
- [51] R. Alaei, C. Rockstuhl, and I. Fernandez-Corbaton, Exact multipolar decompositions with applications, in *Nanophotonics*, *Adv. Opt. Mater.* **7**, 1800783 (2019).
- [52] A. Alú and N. Engheta, How does zero forward-scattering in magnetodielectric nanoparticles comply with the optical theorem?, *J. Nanophotonics* **4**, 041590 (2010).
- [53] W. Liu, A. E. Miroshnichenko, D. N. Neshev, and Y. S. Kivshar, Broadband unidirectional scattering by magneto-electric core-shell nanoparticles, *ACS Nano* **6**, 5489 (2012).
- [54] W. Liu, J. Zhang, B. Lei, H. Ma, W. Xie, and H. Hu, Ultra-directional forward scattering by individual core-shell nanoparticles, *Opt. Express* **22**, 16178 (2014).
- [55] W. Liu, Ultra-directional super-scattering of homogenous spherical particles with radial anisotropy, *Opt. Express* **23**, 14734 (2015).
- [56] D. Sikdar, W. Cheng, and M. Premaratne, Optically resonant magneto-electric cubic nanoantennas for ultra-directional light scattering, *J. Appl. Phys.* **117**, 083101 (2015).
- [57] R. Alaei, R. Filter, D. Lehr, F. Lederer, and C. Rockstuhl, A generalized Kerker condition for highly directive nanoantennas, *Opt. Lett.* **40**, 2645 (2015).
- [58] I. Liberal, I. Ederra, R. Gonzalo, and R. W. Ziolkowski, Superbackscattering from single dielectric particles, *J. Opt.* **17**, 072001 (2015).
- [59] J. Olmos-Trigo, D. R. Abujetas, C. Sanz-Fernández, J. A. Sánchez-Gil, and J. J. Sáenz, Optimal backward light scattering by dipolar particles, *Phys. Rev. Research* **2**, 013225 (2020).
- [60] A. W. Powell, A. P. Hibbins, and J. R. Sambles, Multiband superbackscattering via mode superposition in a single dielectric particle, *Appl. Phys. Lett.* **118**, 251107 (2021).
- [61] R. Gómez-Medina, L. S. Froufe-Pérez, M. Yépez, F. Scheffold, M. Nieto-Vesperinas, and J. J. Sáenz, Negative scattering asymmetry parameter for dipolar particles: Unusual reduction of the transport mean free path and radiation pressure, *Phys. Rev. A* **85**, 035802 (2012).
- [62] B. X. Wang and C. Y. Zhao, Achieving a strongly negative scattering asymmetry factor in random media composed of dual-dipolar particles, *Phys. Rev. A* **97**, 023836 (2018).